Mechanics Research Communications 46 (2012) 41–46

Contents lists available at SciVerse ScienceDirect

Mechanics Research Communications

journal homepage: www.elsevier.com/locate/mechrescom

Hierarchical space frames for high mechanical efficiency: Fabrication and mechanical testing

Daniel Rayneau-Kirkhope[a,*], Yong Mao[a], Robert Farr[b,c], Joel Segal[d]

[a] School of Physics and Astronomy, University of Nottingham, Nottingham, United Kingdom
[b] Unilever R&D, Colworth House, Sharnbrook, Bedford, MK44 1LQ, United Kingdom
[c] London Institute for Mathematical Sciences, 22 South Audley Street, Mayfair, London, United Kingdom
[d] Manufacturing Research Division, Faculty of Engineering, University of Nottingham, Nottingham, United Kingdom

ARTICLE INFO

Article history:
Received 28 April 2011
Received in revised form 14 February 2012
Available online xxx

ABSTRACT

It has been demonstrated theoretically that under certain loading conditions hierarchical structures hold a distinct advantage in efficiency over more conventional designs. Here a particular hierarchical design is studied, and we show that the power-law scaling relations between loading parameters and volume of material required to make a stable structure can be varied systematically. Through computer simulation, we construct mechanism diagrams depicting likely failure modes for a given geometry, which give insight into the optimisation. Using rapid prototyping technologies, the same structure is fabricated and mechanical testing undertaken; the results are compared to theoretical and finite element models.

1. Introduction

Structural hierarchy as a design principle is found throughout nature for highly efficient, multipurpose materials (Baer et al., 1987; Gao et al., 2005; Schaedler et al., 2011; Lakes, 1993). The structure of compact bone, for example, shows structural hierarchy over a range of length scales (Hancox, 1972; Currey, 1984) formed through the tissue's ability to restructure itself in response to prevailing stresses (Currey, 1984). Through its hierarchical construction, high mechanical efficiency is retained while meeting requirements of stiffness (Katz, 1971) and toughness (Piekarski, 1970). Tendons, wood and bamboo also exhibit highly ordered structural hierarchy (Lakes, 1993). Recent theoretical works have shown that through the use of hierarchical design, high mechanical efficiency can be obtained for structures under a range of loading conditions (Rayneau-Kirkhope et al., 2011; Farr and Mao, 2008; Farr, 2007a,b; Murphey and Hinkle, 2003). In the limit of light loading, the optimal number of hierarchical levels increases without bound and the structure becomes fractal on all length scales. Experimental work on hierarchical sandwich panels has confirmed theoretical predictions that second order panels exhibit strength ten times greater than their first order counterparts of the same relative density (Kooistra et al., 2007).

Here, through simulation, we follow the fundamental path of the structure throughout the loading process to analyse the failure of the structure, the results of these simulations support the previously found scaling relationship between compressive loading and volume of material required to make a stable structure (Farr and Mao, 2008). The relationship between failure mode and geometry of a structure is discussed and failure maps are presented for structures with one and two levels of structural hierarchy. Using rapid prototyping technologies an example frame is then constructed and its failure under compressive loading is compared to both freely hinged models and full finite element simulations. The differences between theory and experiment are discussed.

2. Design and basic scaling laws

The structure under investigation is a space frame, constructed through an iterative procedure where the generation, G, of the structure is defined as the number of iterations performed (Farr and Mao, 2008). The generation-1 structure is simply made up of two tetrahedra with n octahedra between them, see Fig. 1(a). The generation-1 structure, when compressively loaded (and initially assuming all beams are pin jointed), has some of its component beams under compression and some under tension. More specifically, the horizontal beams are under tension while all others are under compression. The generation-2 structure is then constructed by replacing all beams in the generation-1 structure that are under compression with scaled generation-1 frames. This procedure is repeated to construct higher order frames, and Fig. 1(b) and (c) show example generation-2 and 3 structures. The naming convention for the parameters that are repeated on different length scales is such that $X_{G,i}$ refers to parameter X in a frame of

* Corresponding author.
E-mail address: ppxdr@nottingham.ac.uk (D. Rayneau-Kirkhope).

0093-6413/$ – see front matter © 2012 Elsevier Ltd. All rights reserved.
http://dx.doi.org/10.1016/j.mechrescom.2012.06.011

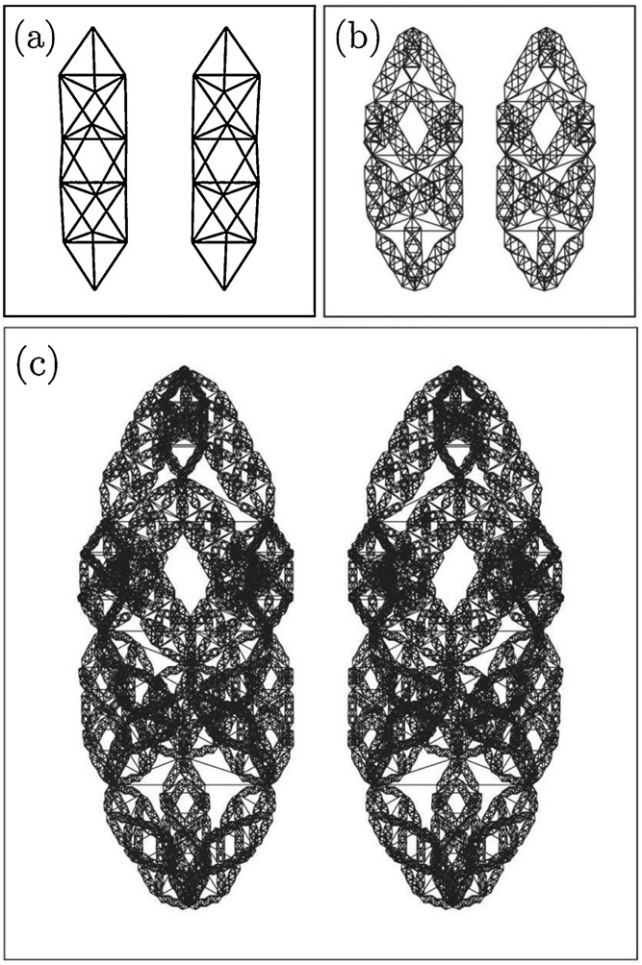

Fig. 1. Example frames of (a) generation-1; (b) generation-2 and (c) generation-3. To view the stereograms in 3D hold the page 20 cm away (30 cm for the lower image) and look through the page, until the images merge.

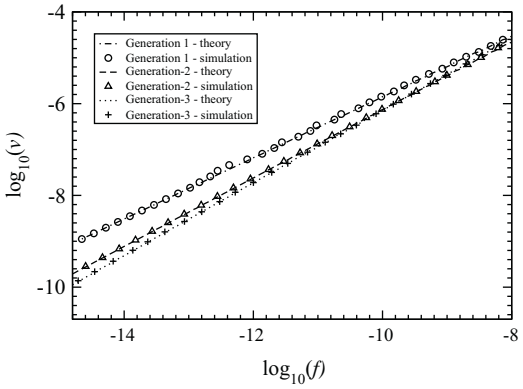

Fig. 2. Scaling of non-dimensionalised volume ν versus the maximum non-dimensionalised loading f for space frames with different generation numbers G. The theoretical results assume that the deformation prior to buckling is very small, while the simulations take this deformations into account, but still yield the same power-law scaling.

generation-G at the ith level. For example, $n_{2,2}$ is the number of octahedra in a generation-2 frame on the longest length scale (which is in part made up of generation-1 substructures), $n_{2,1}$ is the number of octahedra in the substructures of the generation-2 frame (which is constant for all the substructures used at this level). The parameters denoted in this way are number of octahedra in any frame or component structure, $n_{G,i}$; the length of a component beam or structure, $L_{G,i}$; the spring constant of a beam or substructure, $k_{G,i}$ and the force placed through a beam or substructure, $F_{G,i}$. In this notation when $i=0$ the parameter refers to the simple beams that make up the smallest components. Making the assumption that all the component beams are freely hinged at their ends, the failure of each hierarchical level in this structure is decoupled entirely from all others. Thus, under this approximation, the only modes of failure that can interact are those within a single stack of octahedra; in the analytic formulation of this problem, it is assumed either buckling of a single component beam or buckling of the entire (sub-)frame occurs first (Farr and Mao, 2008). In this formulation, therefore, the generation-1 frame has 2 failure modes, failure of a component beam or failure of the entire frame, while a generation-2 frame has 3 failure modes, failure an individual component beam, failure of a subframe of length $L_{2,1}$ or failure of the entire generation-2 frame. Using this approach, through iterative formulae, optimisation of the whole structure can be achieved. The assumption that the failure of each hierarchical level occurs independently of its own substructure can be referred to as a 'continuum' model of the structure (Kooistra et al., 2007). After the optimisation of the structure for the number of octahedra at each hierarchical level and the radius of the component beams, it can be shown that the minimum volume of material (scaled against the length, L, of the structure cubed, $\nu \equiv V/L^3$) required to create a space frame stable under compressive loading F (scaled by the Young's modulus, Y, times by the length of the structure squared, so $f \equiv F/YL^2$) scales as (Farr and Mao, 2008)

$$\nu = \kappa_1(G) f^{(G+1/G+2)}, \tag{1}$$

where $\kappa_1(G)$ is a number which depends on how many generations G are present.

Due to the nature of the $\kappa_1(G)$ dependence on G, it is found that for a given value of loading there is an optimal generation number for the structure which brings about the design of minimal mass. With a decrease in the loading parameter f, the optimal generation number is increased. The optimal generation in realistic situations does not exceed 4, and this, combined with the simple truss construction, makes the implementation of these designs plausible.

3. Scaling laws

First, a computational model (freely hinged) is created to analyse the change in geometry of the structure as it is loaded; such a method predicts the deformation of the structure when loaded gradually and establishes whether the change in loading on the constituent beams is enough to invalidate the continuum assumption and therefore change the scaling law. Plotted in Fig. 2 are the results of these simulations alongside the analytic optimisations against loading showing the dependence of volume with loading and generation as described in Eq. 1. The results of a numerical study in Fig. 2 show that, though the individual beams are found to fail at a lower loading than that predicted analytically, the scaling law is still intact. The results shown in Fig. 2 are for spaceframes as shown in Fig. 1, while the frames fabricated in later sections of this work have the end tetrahedra removed at the highest hierarchical level. It is expected that, under the freely hinged approximation, the geometry changes under loading will not change this scaling relationship, since the change from pin jointed to essentially clamped boundary conditions only affects the largest hierarchical level, and introduces a single pre-factor in the Euler buckling criterion.

The previous analyses (Farr and Mao, 2008) assume that all component beams in the structure fail due to Euler buckling, and that yield of the material is not important in the optimisation procedure. This assumption is shown to be valid in Fig. 3 where the

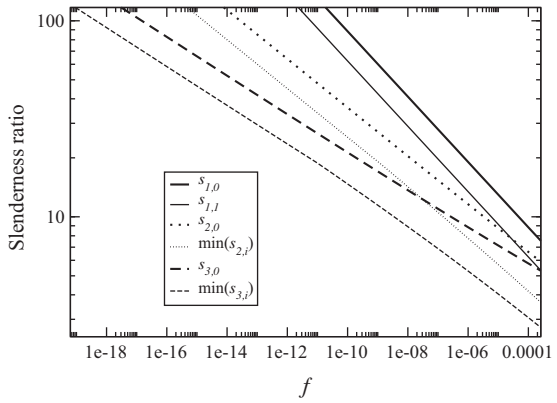

Fig. 3. Slenderness ratio of frames for generation 1–3 against loading parameter for which the frame is optimised. As the loading decreases, the slenderness ratio increases showing where the frames are most efficient it is possible to discount yield as a source of failure of the component beams.

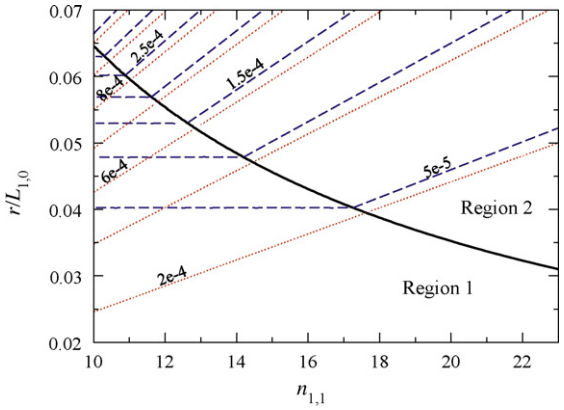

Fig. 4. Through plotting $n_{1,1}$ and $r/L_{1,0}$ we obtain a failure map for the generation-1 structure valid for all values of $L_{1,1}$. The figure is split into two regions; region 1 shows the geometries which lead to failure of the smallest beams in the structure, while region 2 shows where the structure is predicted to fail due to global failure of the frame. The black curve shows the set of optimal geometries. Also shown are contours of constant non-dimensional failure loading ($F/(YL_{1,0}^2)$) separated by values of 5×10^{-5} indicated with (blue on-line) dashed lines and constant non-dimensional volume, $V/L_{1,1}^3$, separated by values of 2×10^{-4} shown in (red on-line) dotted lines. Though here $n_{1,1}$ is shown to take a continuous set of values, in reality only integers values can be realised. (For interpretation of the references to colour in this figure legend, the reader is referred to the web version of the article.)

slenderness ratio of the smallest beams, $s_{G,0}$, is plotted against the loading parameter for which the frame is optimised. Also plotted in Fig. 3 is $\min_{i>0}(s_{G,i})$, where $s_{G,i}$ is the maximal distance from the neutral axis of a (sub)frame to any component part of that (sub)frame for the hierarchical level i divided by $L_{G,i}$; $s_{G,i}$ represents the slenderness of the (sub)frames. We see as the loading parameter becomes smaller, and thus where the frames are most efficient, the slenderness ratio increases.

4. Failure mode

A generation-G structure will have $G+1$ types of failure mode from Euler buckling at each structural level, and it is assumed in the optimisation that each failure mode is independent of the features on different length scales – this is a result of the freely hinged approximation which decouples the failure of one hierarchical level from all others in this class of structures. Through simulation we can construct a failure map of the structures in order to predict which failure mode will be active for a given geometry. As discussed previously, the generation-1 structure has only 2 modes of failure (buckling of the whole structure treated as a single column, and buckling of the individual component beams). Furthermore for a given length $L_{1,1}$ of structure,the geometry is fully defined by $r_{1,1}$ and $n_{1,1}$, so by plotting the amount of material used as a function of these two parameters we can predict the mode of failure of any given (non-optimal) design, and so obtain the unique optimal design. Fig. 4 shows the evolution of the optimal design with varying loading criteria: as the value of loading decreases, the number of octahedra in the optimal design increases and the radii of the beams decrease.

The generation-2 structure has 3 classes of failure mode. For a given volume, V, and length of structure, $L_{2,2}$, we can plot $n_{2,2}$ and $n_{2,1}$ which then fully define the structure; it should be noted in the resulting plot [Fig. 5] that the parameter r varies in order to keep V constant. For a given volume the optimal construction is found when the structure is on the point of failure on all length scales, and contours of constant loading failure are also shown in the figure.

5. Fabrication and testing

To test the structure, the largest length scale tetrahedra at each end are replaced with planar surfaces, which provides a more suitable mechanical coupling; through this adaptation loading eccentricities will be reduced. The structure was fabricated through rapid prototyping on an EnvisionTEC perfactory machine (EnvisionTEC, 45968 Gladbeck, Germany) using EnvisionTEC RC25 (NanoCure) material and a second set manufactured on the same machine using EnvisionTEC R05 material. Each structure has dimensions of approximately 40 mm × 11 mm × 11 mm including the end plates. The dimensions of the smallest struts within the structure were approximately 1.35 mm long with radius of 0.15 mm, Fig. 6 shows part of an example structure. The build process using the RC25 (NanoCure) material was undertaken using two different layer thicknesses, 35 μm and 50 μm while the R05 material was manufactured using a layer thickness of 25 μm. The difference in performance of the structures is analysed in Section 7. The compression tests are undertaken at a constant compression rate while the reaction forces are measured; the compression

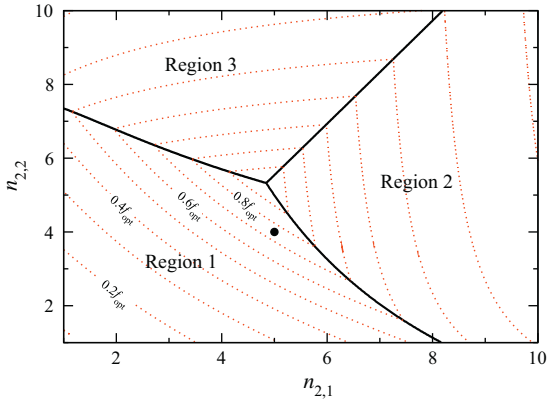

Fig. 5. Showing the predicted mode of failure for an adapted generation two structure with non-dimensional volume of $v = 9.3 \times 10^{-3}$ and an optimal failure loading parameter of $f_{opt} = 3.07 \times 10^{-3}$. The area of the plot is separated into 3 regions, region 1 shows the values of $(n_{2,1}, n_{2,2})$ where the smallest solid beams in the structure will fail first, region 2 is such that the substructure generation-1 frames will fail first, and region 3 shows the parameters which put the generation-2 frame of length $L_{2,2}$ fail first. The dotted lines (red on-line) show the contours of constant failure at loading which are separated by 0.1 times the optimal loading value. The black circle shows the geometry of the structure manufactured here. In the construction of space frames, $n_{2,2}$ and $n_{2,1}$ are restricted to the integers. (For interpretation of the references to colour in this figure legend, the reader is referred to the web version of the article.)

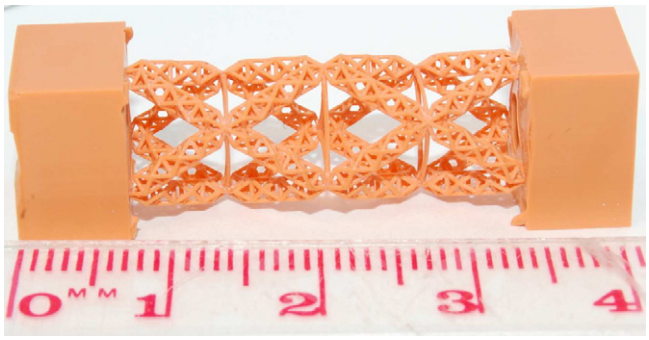

Fig. 6. The generation-2 frame. The final frame was built without the top tetrahedron and with a plate attached to both top and bottom to allow reliable compression tests to be undertaken.

rate for all compression tests is 1.2 $\mu m\,s^{-1}$ using an Instron 5569 machine, Fig. 7 shows the set up used.

6. Results

Due to the manufacturing process, the material has a clearly visible layered texture [see Figs. 8 and 12]. This leads to anisotropic material performance under stress and different behaviour of the material to that observed when testing its bulk properties (EnvisionTEC). In analysing our compression results we have introduced an 'Effective Young's Modulus,' Y_{eff} of the material to compensate for the altered performance of the structure due to the layering effect. The Effective Young's Modulus is taken such that the deformation of the structure at very small displacements is in line with the results of finite element simulations. The normalised results are then plotted in Figs. 9 and 10 for frames manufactured in both the R05 and the RC25 (NanoCure) materials along side the theoretical result with a linear displacement assumption, the freely hinged model which neglects bending effects of the beam, and a full finite element simulation of the structure. This analysis is undertaken using ANSYS 13.0. A linear buckling analysis precedes a full non-linear analysis using inbuilt routines. The difference between

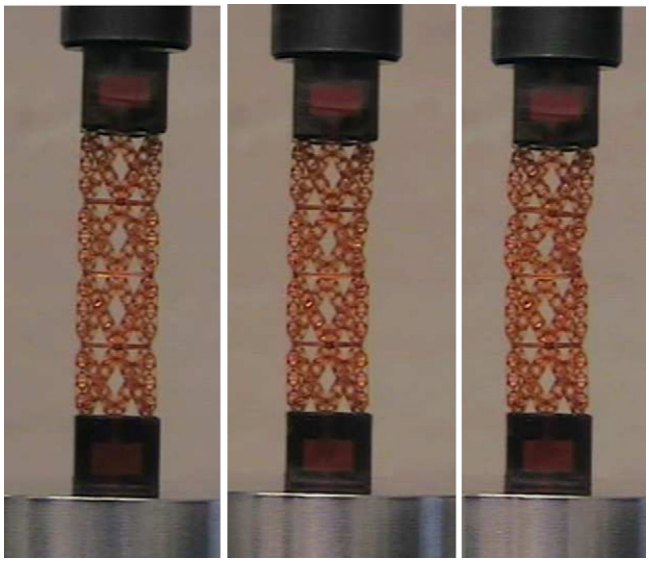

Fig. 7. The setup used for the compression tests and the modified structure with end tetrahedra replaced by planar surface. Structures in compression tests shown are those made out of R05 and images taken at 3 different time intervals: the first is before loading. The second at the point of first failure, where the second substructure from the top is seen to be deformed (due to failure of a smaller component beam). In the third image the deformation is seen throughout the top half of the structure.

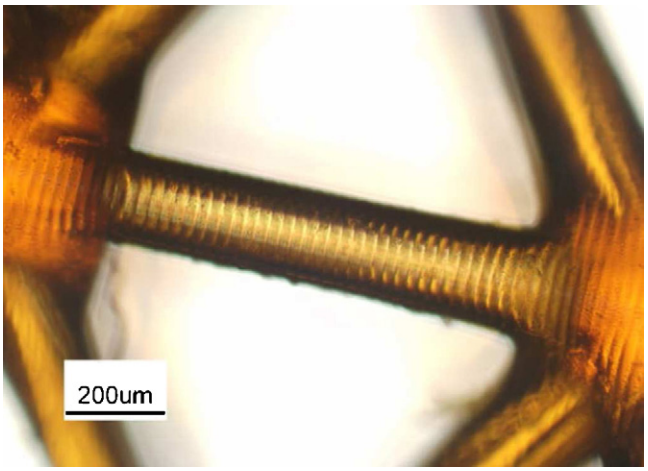

Fig. 8. Close-up of the structure of Fig. 6. The layering of the R05 material is clearly visible in this microscope image. Image taken using a Nikon Optiphot at a magnification of ×10. The image also clearly shows the extra material deposited around the joints.

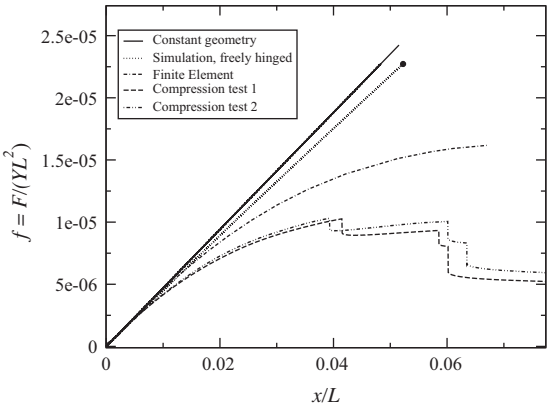

Fig. 9. The results of the compression tests for two structures made from the RC25 (NanoCure) material with layer thickness 35 μm against theory and simulations. The black circle indicates where the freely hinged model would fail due to fracture of the tension beams of length $L_{2,1}$ in accordance with the material properties; the structure reaches the point of failure due to the breaking of the long tension beams just before the smallest beams in the structure buckle.

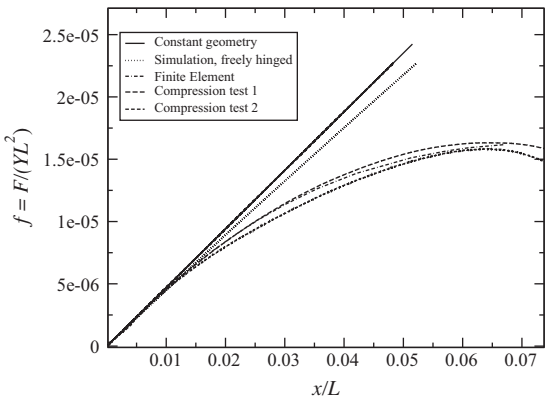

Fig. 10. The results of the compression tests for two structures manufactured using R05 with layer thickness 25 μm against theory and simulations. The failure here is due to the smallest beams in the structure failing by buckling.

the linear analysis and the maximum loading of the path shown in Figs. 9 and 10 is found to be approximately 35%. In both cases appropriate boundary conditions are taken into account for the modified structure with the largest tetrahedra removed from the frame (as shown in Fig. 6). The scaling of f and x/L is such that the finite element analysis curves plotted in Figs. 9 and 10 do not change between the materials with different Y values, the Poisson ratio of the material is taken to be 0.3. In both cases, the failure point of the finite element curve indicates a loss of elastic stability. In mechanical testing, it is found that for the frame constructed using the RC25 (NanoCure) material the failure occurs through breaking of the longer tension beams in the structure, these breaks are represented by vertical steps in the path of displacement against load for the compression tests in Fig. 9. Taking into account the failure under tension at 2.5% elongation (bulk material properties) we show this failure mode is predicted to occur first in the freely hinged model (see Fig. 9) however it is not predicted in the finite element simulations (the finite element simulation predicts a maximal elongation of the tension beams of 1.8%). It is understood that the layered nature of the material due to the manufacturing process will have a greater effect on failure due to tension, as any lack of adhesion between the layers will have an amplified effect when placed under tension. The R05 material can withstand an elongation great enough to test the failure mode predictions from buckling made previously. Fig. 5 shows that failure due to the smallest beams should be the active mode. This is indeed found to be the case in experiment giving qualitative agreement between theory and experiment.

The value of Y_{eff} differs depending on the layer thickness. We have found that the values of Y_{eff} for the RC25 (NanoCure) material are:

$$Y_{\text{eff}} = 2.2\,\text{GPa} \pm 0.1 \tag{2}$$

$$Y_{\text{eff}} = 1.5\,\text{GPa} \pm 0.05 \tag{3}$$

for layer thicknesses of 50 μm and 35 μm respectively. While the value of Y_{eff} for the R05 material with layer thickness of 25 μm is found to be

$$Y_{\text{eff}} = 0.5\,\text{GPa} \pm 0.1. \tag{4}$$

7. Discussion

We see from Fig. 10 that the deformation of the R05 structure is very close to that predicted by the finite element simulation; in the case of the RC25 (NanoCure) material, Fig. 9, both the strain at failure and the deformation at failure is much lower than predicted by these models. This difference in behaviour can be attributed to the different nature of the failure in the two materials and the layered texture of the material giving inhomogeneous behaviour under tension in particular. The loading at failure in both cases differs significantly from the freely hinged results. This difference must be investigated further to establish if the addition of bending moments at the beam ends is enough to invalidate the previously found scaling laws.

It is noted that the deformation of the structure as predicted by the simple freely hinged model method agrees with the full finite element model very well until the loading reaches a threshold value and the effects of bending moments at the end of the beams become important. When the structure is tested physically we see that this proportional limit is shifted to a lower value of the loading parameter for the RC25 (NanoCure). This can be explained through the presence of excess material around the joint and the non-uniform beam thickness. The difference between the freely hinged model and the finite element simulation is down to the beams being modelled as free to hinge at the joints in the former and not in the latter.

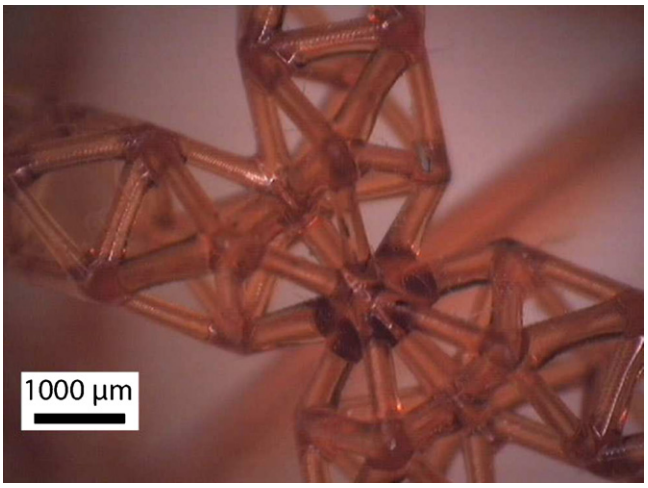

Fig. 11. The joints of the frame have excess material around them which contributes the differences between simulation and the test results. This is particularly apparent in the R05 material.

The difference between the actual testing can, in part, be attributed to an amplification in this effect due to the excess material where beams meet. This excess material is shown clearly in Fig. 11. We see good agreement between the finite element simulation and the physical testing of the structure made using R05 material. It is also important to note that any imperfections in the material will be amplified by the structure's dependence on structural elements much smaller than its own length. The nature of the RC25 (NanoCure) material is such that failure is due to the breaking of the beams loaded under tension rather than any of the compression beams failing – although this does not invalidate the 'continuum' approximation (Fig. 12).

In summary, we have designed optimal hierarchical space frames based on freely hinged couplings between component beams, and then performed finite element simulations and physical measurements on structures to find the failure modes once this freedom at the joints is removed. Despite potential non-uniformity of the resins used to make the physical structures, the finite element analysis agrees well with the experimental results on the R05 material (although R25 is brittle under tension and so gives less good agreement). However, the analysis of freely hinged structures predicts that they will fail at higher compression forces and lower strains than are obtained by finite element analysis (and experi-

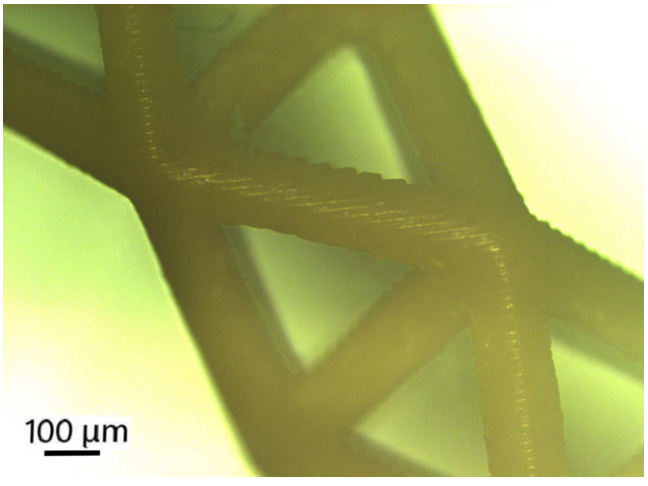

Fig. 12. The RC25 (NanoCure) material clearly showing the layering effect of the manufacturing process on the structures surface and a more opaque appearance.

ment) without freely hinged joints. In future we would therefore like to investigate the optimal form of non-freely hinged hierarchical space frames, and determine whether the scaling laws for the material required to support a given compression force that apply to the freely hinged case still hold true.

Acknowledgements

The authors wish to thank the work of Fred Grillet, Ranbir Singh Ghatoura and Mark Strickland of the Engineering Department at the University of Nottingham.

Appendix A. Fabrication

The structures tested here were fabricated using a modified EnvisionTEC Perfactory® type III mini system. This mask-projection based photopolymerisation system has a 2800×2100 pixel digital light processing projector allowing a resolution of $5\,\mu m$. The structure manufactured here was first modelled as an STL file as a 3D structure, before being split into its component 2D layers of a given thickness and stored as a job file using Perfactory RP proprietary software. Light with wavelength approximately 475 nm is then passed through the projector and focused onto the resin surface for polymerisation of the exposed areas. The sample is then washed using ispropanol in an ultrasonic bath and left to dry. For the structures made from R05 a postcuring procedure is followed using an EnvisionTEC Otoflash System to harden the material.

Appendix B. 3D Printing

With the ever increasing capabilities of additive manufacturing and the realistic possibility 3D printing being bought into a more public domain the authors feel that the STL file for the frame constructed here should be made freely available. The STL file therefore is freely available as supplementary material on-line.

Appendix C. Supplementary data

Supplementary data associated with this article can be found, in the online version, at doi:http://dx.doi.org/10.1016/j.mechrescom.2012.06.011.

References

Baer, E., Hiltner, A., Keith, H.D., 1987. Science 235, 1015.
Currey, J., 1984. The Mechanical Adaptations of Bones. Princeton, New Jersey.
'envisionTEC RC25 (NanoCure) Technical Data', 22 November 2010. 'www.envisiontec.de'.
'envisionTEC R05 and R11 Technical Data', 22 November 2010. 'www.envisiontec.de'.
Farr, R.S., Mao, Y., 2008. EPL 84, 14001.
Farr, R.S., 2007a. Phys. Rev. E 76, 046601.
Farr, R.S., 2007b. Physical Review E 76, 056608.
Gao, H., Wang, X., Haimin, Y., Stanislav, G., Eduard, A., 2005. Mechanics of Materials 37, 275–285.
Hancox, N.M., 1972. Biology of Bone. Cambridge University Press.
Katz, J.L., 1971. Biomechanics 4, 455–473.
Kooistra, G.W., Deshpande, V., Wadley, H.N.G., 2007. Journal of Applied Mechanics 74, 259–268.
Lakes, R., 1993. Nature 361, 511–515.
Murphey, T., Hinkle, J., 2003. 44th AIAA/ASME/ASCE/AHS/ASC Conference , Norfolk, VA, April 7–10, p. 1903.
Piekarski, K., 1970. Journal of Applied Physics 41, 215–223.
Rayneau-Kirkhope, D., Farr, R.S., Mao, Y., 2011. EPL (93), 34002.
Schaelder, T.A., Jacobsen, A.J., Torrents, A., Sorensen, A.E., Lian, J., Greer, J.R., Valdevit, L., Carter, W.B., 2011. Science 334, 962–965.